

Sensitized-RANS Modelling of Turbulence: Resolving Turbulence Unsteadiness by a (Near-Wall) Reynolds Stress Model

Suad Jakirlić and Robert Maduta

Abstract A turbulence model designed and calibrated in the steady RANS (Reynolds-Averaged Navier-Stokes) framework has usually been straightforwardly applied to an unsteady calculation. It mostly ended up in a steady velocity field in the case of confined wall-bounded flows; a somewhat better outcome is to be expected in globally unstable flows, such as bluff body configurations. However, only a weakly unsteady mean flow can be returned with the level of unsteadiness being by far lower compared to a referent database. The latter outcome motivated the present work dealing with an appropriate extension of a near-wall Second-Moment Closure (SMC) RANS model towards an instability-sensitive formulation. Accordingly, a Sensitized-RANS (SRANS) model based on a differential, near-wall Reynolds stress model of turbulence, capable of resolving the turbulence fluctuations to an extent corresponding to the model's self-balancing between resolved and modelled (unresolved) contributions to the turbulence kinetic energy, is formulated and applied to several attached and separated wall-bounded configurations—channel and duct flows, external and internal flows separating from sharp-edged and continuous curved surfaces. In most cases considered the fluctuating velocity field was obtained started from the steady RANS results. The model proposed does not comprise any parameter depending explicitly on the grid spacing. An additional term in the corresponding length scale-determining equation providing a selective assessment of its production, modelled in terms of the von Karman length scale (formulated in terms of the second derivative of the velocity field) in line with the SAS (Scale-Adaptive Simulation) proposal (Menter and Egorov, *Flow Turbul Combust* 85:113–138, (2010) [14]), represents here the key parameter.

S. Jakirlić (✉) · R. Maduta

Institute of Fluid Mechanics and Aerodynamics / Center of Smart Interfaces, Technische Universität Darmstadt, Alarich-Weiss-Straße 10, 64287 Darmstadt, Germany
e-mail: s.jakirlic@sla.tu-darmstadt.de

R. Maduta

Outotec GmbH, Ludwig-Erhard-Strasse 21, 61440 Oberursel, Germany
e-mail: roberttibor@gmx.li

1 Introduction

The work on development of the hybrid RANS/LES (Large-Eddy Simulation) methods and novel Unsteady RANS (URANS) methods (RANS model plays here the role of a sub-scale model) has been greatly intensified in recent years. The relevant methods have been proposed by Spalart et al. ([20], DES—Detached Eddy Simulation; see Spalart, [19] for the DES method upgrades, namely Delayed DES and Improved Delayed DES), Menter and Egorov ([14]; SAS—Scale-Adaptive Simulations), Girmaji ([7]; PANS—Partially Averaged Navier Stokes; see also Basara et al. [1], for the PANS method extension to account for the near-wall effects), and Chaouat and Schiestel ([4]; PITM—Partially Integrated Transport Model). The common feature of all these models is an appropriate modification of the scale-determining equation providing a dissipation rate level which suppresses the turbulence intensity towards the subgrid (i.e. sub-scale) level in the regions where large coherent structures with a broader spectrum dominate the flow, allowing in such a way evolution of structural features of the associated turbulence. Whereas an appropriate dissipation level enhancement in the PANS method (similar is in the case of the PITM method) is achieved by reducing selectively (e.g. in the separated shear layer region) the destruction term in the model dissipation equation, i.e. its coefficient $C_{\varepsilon,2}$ (e.g. the grid-spacing-dependent model coefficient function in the PANS method provides appropriate decrease of the standard value $C_{\varepsilon,2} = 1.92$, prevailing in the near-wall region, towards a significantly lower value in the separated shear layer of the periodic 2D hill flow, see e.g. [3]), an additional production term was introduced into the ω equation ($\omega \propto \varepsilon/k$ —inverse turbulent time scale) in the SAS framework. This term is modelled in terms of the von Karman length scale comprising the second derivative of the velocity field ($\nabla^2 \mathbf{U}$), which is capable of capturing the vortex size variability, [14].

The work reported here aims at developing an instability sensitive, anisotropy-resolving Second-Moment Closure (SMC) model. This model scheme, functioning as a ‘sub-scale’ model in the Unsteady Sensitized-RANS (SRANS) framework, represents a differential near-wall Reynolds stress model formulated in conjunction with the scale-supplying equation governing the homogeneous part of the inverse turbulent time scale: $\omega_h = \varepsilon_h/k$. The model capability to account for the vortex length and time scales variability was enabled through a selective enhancement of the production of the dissipation rate in line with the SAS proposal (Scale-Adaptive Simulation, Menter and Egorov, [14]) pertinent particularly to the highly unsteady separated shear layer region. The predictive performances of the proposed model are checked by computing series of internal and external, two-dimensional and three-dimensional flows in channels, ducts and past bluff bodies including separation from sharp-edged and continuous curved surfaces in a range of Reynolds numbers.

2 Computational Method

The following section briefly outlines the computational model proposed. It is followed by description of the numerical method and associated details.

2.1 Computational Model

The equation governing the homogeneous part of the total viscous dissipation rate, $\varepsilon_h = \varepsilon - 0.5\nu\partial^2 k/(\partial x_j \partial x_j)$, modelled in term-by-term manner by Jakirlic and Hanjalic [8] represents the starting point for the present development. The RSM-based ω_h -equation following directly from the ε_h -equation (here, instead of originally used General-Gradient-Diffusion-Hypothesis (GGDH) for the turbulent diffusion modelling, the Simple GDH with diffusion coefficient modelled in terms of turbulence viscosity was applied; thereby, no difference between the Prandtl-Schmidt numbers corresponding to the quantities k and ε_h was made; $\sigma_k = \sigma_\varepsilon = \sigma_\omega = 1.1$ is adopted finally) by using well-known relationship

$$\frac{\mathbf{D}\omega_h}{\mathbf{D}t} = \frac{1}{k} \frac{\mathbf{D}\varepsilon_h}{\mathbf{D}t} - \frac{\varepsilon_h}{k^2} \frac{\mathbf{D}k}{\mathbf{D}t} \quad (1)$$

with

$$\frac{\mathbf{D}k}{\mathbf{D}t} = \frac{\partial}{\partial x_k} \left[\left(\frac{1}{2}\nu + \frac{\nu_t}{\sigma_k} \right) \frac{\partial k}{\partial x_k} \right] + P_k - \varepsilon_h \quad \text{and}$$

$$\frac{\mathbf{D}\varepsilon_h}{\mathbf{D}t} = \frac{\partial}{\partial x_k} \left[\left(\frac{1}{2}\nu + \frac{\nu_t}{\sigma_\varepsilon} \right) \frac{\partial \varepsilon_h}{\partial x_k} \right] + C_{\varepsilon,1} \frac{\varepsilon_h}{k} P_k - C_{\varepsilon,2} \frac{\varepsilon_h \varepsilon_h}{k} + 2C_{\varepsilon,3} \nu \nu_t \frac{\partial^2 U_i}{\partial x_j \partial x_l} \frac{\partial^2 U_i}{\partial x_j \partial x_l}$$

reads:

$$\begin{aligned} \frac{\mathbf{D}\omega_h}{\mathbf{D}t} = & \frac{\partial}{\partial x_k} \left[\left(\frac{1}{2}\nu + \frac{\nu_t}{\sigma_\omega} \right) \frac{\partial \omega_h}{\partial x_k} \right] + C_{\omega,1} \frac{\omega_h}{k} P_k - C_{\omega,2} \omega_h^2 \\ & + \frac{2}{k} \left(C_{cr,1} \frac{1}{2}\nu + C_{cr,2} \frac{\nu_t}{\sigma_\omega} \right) \frac{\partial \omega_h}{\partial x_k} \frac{\partial k}{\partial x_k} + \frac{2}{k} C_{\omega,3} \nu \nu_t \frac{\partial^2 U_i}{\partial x_j \partial x_l} \frac{\partial^2 U_i}{\partial x_j \partial x_l} \end{aligned} \quad (2)$$

with $P_k = -\overline{u_i u_j} \partial U_i / \partial x_j$ representing production of the kinetic energy of turbulence and coefficients $C_{\omega,1} = C_{\varepsilon,1} - 1 = 0.44$, $C_{\omega,2} = C_{\varepsilon,2} - 1 = 0.8$ and $C_{\omega,3} = 1.0$ taking their standard values. The introduction of the ‘correction’ coefficients $C_{cr,1} = 0.55$ and $C_{cr,2} = 0.275$ into the cross-derivative term copes with the correction of the near-wall behaviour of the ω_h -variable (see [9] for more details). Last term on the right-hand side represents the gradient production term; here, instead of the original formulation (modelled by using the vorticity transport theorem)

comprising both the mean rate of strain and second derivative of the velocity field a simplified version (pertinent to an eddy-viscosity model) is applied in line with the request for a practical model usage. The model for turbulent viscosity ν_t , accounts for both Reynolds stress anisotropy (being beyond the reach of the eddy-viscosity model group) and viscosity effects, with characteristic length representing a switch between the Kolmogorov length scale and the turbulent length scale.

The latter equation is appropriately extended through the introduction of the SAS term [14] into the ω_h -equation:

$$\begin{aligned} \frac{\mathbf{D}\omega_{h,SAS}}{\mathbf{D}t} &= \frac{\mathbf{D}\omega_h}{\mathbf{D}t} + P_{SAS}; \quad P_{SAS} = C_{RSM,1} \max[P_{SAS}^*, 0] \\ P_{SAS}^* &= 2.3713\kappa S^2 \left(\frac{L}{L_{vk}}\right)^{1/2} - 3C_{RSM,2}k \max\left[\frac{(\nabla\omega_h)^2}{\omega_h^2}, \frac{(\nabla k)^2}{k^2}\right] \end{aligned} \quad (3)$$

with $L = k^{1/2}/\omega_h$ being the turbulent length scale, $L_{vk} = \kappa S/|\nabla^2 U|$ (with $\nabla^2 U = [\partial^2 U_i/\partial x_j^2 \times \partial^2 U_i/\partial x_j^2]^{1/2}$) representing the 3D generalization of the classical boundary layer definition of the von Karman length scale and S the invariant of the mean strain tensor ($S = \sqrt{2S_{ij}S_{ij}}$; $S_{ij} = 0.5(\partial U_i/\partial x_j + \partial U_j/\partial x_i)$). It should be noted that the P_{SAS} term introduced in the ω_h -equation has almost identical form as the one being used in the eddy-viscosity-based $k - \omega$ SST-SAS model [14]. However, two coefficients, $C_{RSM,1} = 0.004$ and $C_{RSM,2} = 8$ and exponent of the length scales ratio ((1/2) instead of 2) are introduced adjusting its use in the framework of a Second-Moment Closure model. The natural decay of the homogeneous isotropic turbulence, fully developed channel flows in a range of Reynolds number (with underlying velocity field following the logarithmic law) and the non-equilibrium 2D hill flow at two different Reynolds numbers ($Re_H = 10,600$ and $37,000$) have been interactively computed in the process of the coefficients calibration. Equation (3) represents a grid-spacing-free formulation. This explicit non-dependence on the grid-spacing represents certainly an advantage over some hybrid LES/RANS models, especially in the case of unstructured grids with arbitrary grid-cell topology. The contours of the P_{SAS} term in the flow over a periodical arrangement of 2D hills and past a tandem cylinder configuration depicted in Fig. 1 clearly shows that it is active only in the region of the separated shear layer. In the reminder of the flow domain, especially in the near-wall regions, its effect vanishes.

The proposed model is solved in conjunction with the Jakirlic and Hanjalic's [8] Reynolds stress model equation ($\varepsilon_h = \omega_h k$, $k = \overline{u_i u_i}/2$, $P_{ij} = -\overline{u_i u_k} \partial U_j / \partial x_k - \overline{u_j u_k} \partial U_i / \partial x_k$); similar to the scale-supplying equation (Eq. 2) the GGDH turbulent diffusion model is replaced by the corresponding SGD model formulation:

$$\frac{\partial \overline{u_i u_j}}{\partial t} + \frac{\partial U_k \overline{u_i u_j}}{\partial x_k} = \frac{\partial}{\partial x_k} \left[\left(\frac{1}{2} \nu + \frac{\nu_t}{\sigma_{\overline{u_i u_j}}} \right) \frac{\partial \overline{u_i u_j}}{\partial x_k} \right] + P_{ij} - \varepsilon_{ij}^h + \Phi_{ij} + \Phi_{ij}^w \quad (4)$$

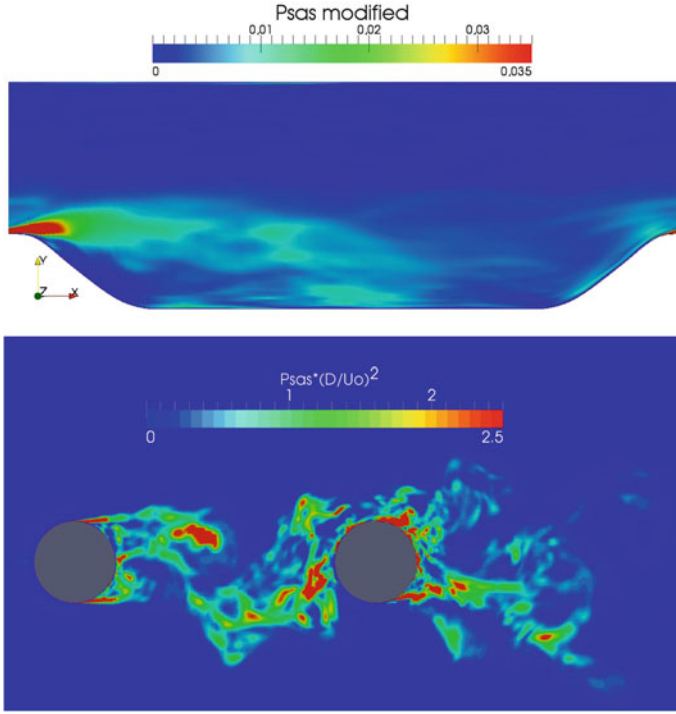


Fig. 1 Contours of the P_{SAS} term (Eq. 3) coloured by its magnitude in the 2D hill flow (*upper*) and flow past a tandem-cylinder (*lower*)

For more detailed insight into the modelling rationale interested readers are referred to [9].

2.2 Numerical Method

All computations were performed using the code Open-FOAM, an open source Computational Fluid Dynamics toolbox (www.open CFD.co.uk/openfoam), utilizing a cell-center-based finite volume method on an unstructured numerical grid and employing the solution procedure based on the implicit pressure algorithm with splitting of operators (PISO) for coupling between pressure and velocity fields. SIMPLE procedure was applied when computing the steady flows using the RANS-RSM model. The convective transport was discretized by a scheme blending between the second order central differencing (CDS) and first order upwind (UDS) schemes with $\gamma_{CDS} = 0.95$ and $\gamma_{UDS} = 0.05$ in most of the cases considered. For the time integration the second order three point backward scheme was used. The code is parallelized applying the Message Passing Interface (MPI) technique for communication between the processors.

3 Results and Discussion

The predictive performances of the proposed instability-sensitive Reynolds stress model (denoted by IS-RSM throughout the work) are intensively assessed in numerous aerodynamic-type flows of different complexity featured also by 2D and 3D separation along with available experimental, DNS (Direct Numerical Simulation) and LES reference results: fully developed flow in a plane channel, flow over a series of axisymmetric 2D hills, flow over a backward-facing step, flow over a wall-mounted fence, flow in a three-dimensional diffuser and flow past tandem cylinder configurations. Figures 2, 3, 4, 5, 6, 7, 8, 9, 10, 11 and 12 display exemplarily some selected results obtained by the consequent models application. For purpose of the mutual comparison the results of the ‘background’ RANS-RSM model are also depicted. For more extensive result presentation and more detailed discussion, also with respect to the computational issues, interested readers are referred to [9].

3.1 Fully Developed Flow in a Plane Channel

Fully developed turbulent flow in a plane channel represents most important representative of wall-bounded flow configurations for studying wall proximity effects on turbulence structure characterized by enhanced anisotropy of both the Reynolds stress tensor and stress dissipation tensor. Channel flow represents a globally stable, unidirectional (in mean) flow ($\partial/\partial x_1 = 0$, $\partial/\partial x_3 = 0$) characterized by a strong mean shear ($\partial U_1/\partial x_2$) but with a low level of inherent forcing. In such a flow, the employment of conventional RANS models, especially those on the second-moment closure level, leads traditionally to correctly predicted distribution of the Reynolds stress components and mean velocity. Accordingly, capturing the turbulence instabilities is here not of decisive importance (as e.g. in the flow over a 2D hill). However, as the consequence of the enhanced sensitivity to turbulence unsteadiness, appropriate eddy-structure resolving is enabled also in such a globally stable flow configuration.

Figure 2-left illustrates the instantaneous flow field obtained by the present instability-sensitive model starting from the mean flow and turbulence fields obtained by the RSM model within the steady RANS framework (periodic inlet/outlet boundary conditions have been applied with the streamwise pressure gradient imposed in accordance with the relevant Reynolds number). Presently, friction-velocity-based Reynolds number $Re_\tau = 395$ is considered; reference DNS database is from [15]. The solution domain adopted ($L_x \times L_y \times L_z = 4h \times 2h \times 2h$); with h representing the half channel width) was meshed by a grid comprising 462,000 ($N_x \times N_y \times N_z = 70 \times 110 \times 60$) grid cells, implying the near-wall resolution in terms of the height of the wall-next grid cell corresponding to $\Delta y^+ = 1.6$. Figure 2-right shows the modelled and resolved fractions of the streamwise and shear Reynolds stress components obtained using the present IS-RSM model. The maximum ratio of the modelled to total kinetic energy related to both turbulent stress components corresponding approximately to 25 % is found in the near-wall region.

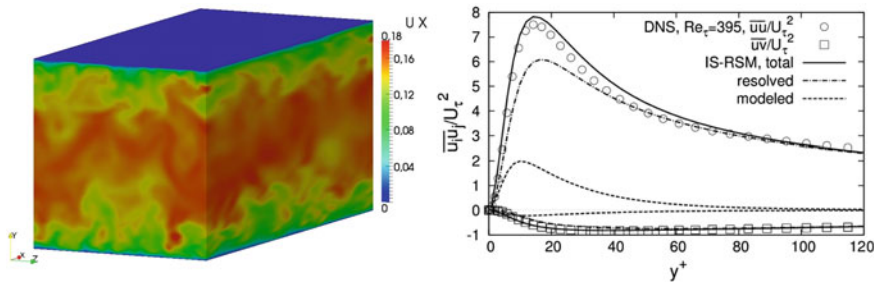


Fig. 2 Fully developed flow in a plane channel at $Re_\tau = 395$ —instantaneous axial velocity field obtained by the present IS-RSM (*left*) and the streamwise ($\overline{u^2}$) and shear (\overline{uv}) Reynolds stress components (*right*); DNS from [15]

3.2 Periodic Flow Over a 2D Hill

Flow over a series of the hill-shaped constrictions (reference LES results have been made available by Fröhlich et al. [6] and Breuer et al. [2]; complementary experimental investigations have been performed by Rapp and Manhart, [18]) exhibits a number of features typically associated with a separating flow: boundary layer separation from a continuous curved surface, reattachment, highly unsteady shear layer that separates the main stream from the recirculation flow, relaxation in the post-reattachment region, alternating adverse (flow deceleration) and favourable (flow acceleration) pressure gradient effects (globally along the flow but even across the same streamwise location), strong departure from the equilibrium conditions, streamline curvature effects, wall proximity effects, Reynolds stress anisotropy, etc. This flow configuration is characterized by high level of natural instability, originating primarily from the highly intermittent separation region oscillating over a wider wall area. Consequently, a highly unsteady separated shear layer spread over a larger portion of the flow domain was generated. Accordingly, it could be concluded without going into greater details that the correct capturing of the present 2D-hill flow configuration is beyond the reach of the conventional, inherently steady RANS closures, almost independent of the modelling level (the complementary RANS-RSM results are also illustrated). The incapability of accounting for any spectral dynamics makes RANS closures limited for capturing correctly such flows dominated by large-scale dynamics. A direct consequence is inadequate (low) level of turbulence activity (controlling the reattachment process) in the separated shear layer and correspondingly longer recirculation zone (see e.g., Fig. 4). The solution domain (with dimensions $(L_x, L_y, L_z) = (9H, 3.03H, 4.5H)$), see Fig. 3-left, is in accordance with the reference LES simulation. The mesh consisting of $N_x \times N_y \times N_z = 160 \times 160 \times 60$ grid cells was designed by an appropriate coarsening of the 13 Mio. cells fine grid made available by Breuer et al. [2]. Both the $Re_H = 10,600$ case and the $Re_H = 37,000$ case (the mean velocity and Reynolds stress results of the former case are not shown here due to sake of brevity—these are of the similar quality) were computed using the same mesh (lower Re-number case was computed also by using a substantially

coarser grid— $N_x \times N_y \times N_z = 80 \times 100 \times 30$ —no important difference in results was obtained). Similar to the fully developed channel flow (previous section), periodic inlet/outlet boundary conditions have been utilized with the streamwise pressure gradient corresponding to the prescribed Reynolds number. It is interesting to report that no initial turbulence fluctuations were necessary in this periodical flow configuration. The mean flow and turbulent quantities obtained by the steady RANS computations using the background $\overline{u_i u_j} - \omega_h$ model served for the initialization of the computations with the present IS-RSM formulation.

The results obtained by computing the 2D hill configuration, displayed in Fig. 3-left, document appropriate vortex structure reproduction—visualized here by the instantaneous velocity field—being beyond the reach of any RANS model. The introduction of the P_{SAS} -term (Eq. 3) within the instability sensitive second-moment closure in the Unsteady RANS framework contributed strongly to the turbulence activity intensification (originating from the resolved motion) in the region around the separation point (see the P_{SAS} -field in Fig. 1-upper). The model capability to account for the large-scale structures and bulk unsteadiness led consequently to the increased magnitude of the turbulent shear stress component (Fig. 4-lower; typical result pertinent to any RANS model is a significantly lower turbulence intensity in the separated shear layer; for comparison, the results of the RANS computations by the $\overline{u_i u_j} - \omega_h$ model denoted by RSM are also displayed), improved shape of the mean velocity profiles (Fig. 4-upper) and correctly predicted reattachment length, Figs. 3-right and 5. The latter figures illustrate appropriate recirculation zone shortening, from $(x/H)_{RP} = 4.62$ (pertinent to the lower Reynolds number $Re_H = 10,600$) towards $(x/H)_{RP} = 3.72$ (pertinent to the higher Reynolds number $Re_H = 37,000$) in good agreement with the LES ($(x/H)_{RP} = 4.62$) and experimental ($(x/H)_{RP} = 3.76$) reference results.

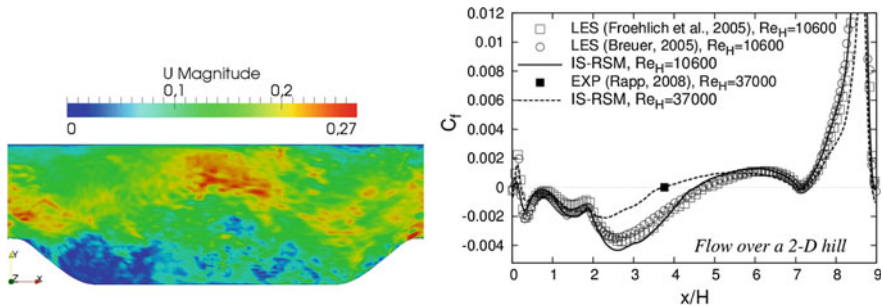


Fig. 3 Periodic flow over a 2D hill: instantaneous velocity field obtained by the present IS-RSM at $Re_H = 10,600$ (left) and friction coefficient development at the lower wall for both Reynolds numbers considered (right)

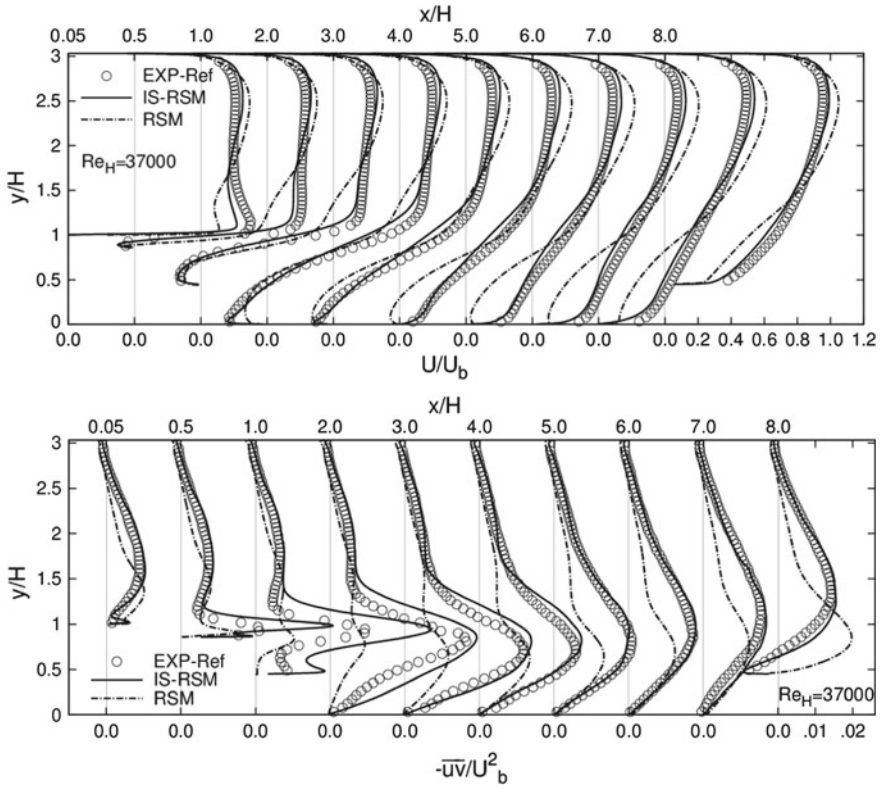


Fig. 4 Periodic flow over a 2D hill at $Re_H = 37,000$ —mean velocity (*upper*) and shear stress component (*lower*) profile developments obtained by the present IS-RSM; Exp. from [18]

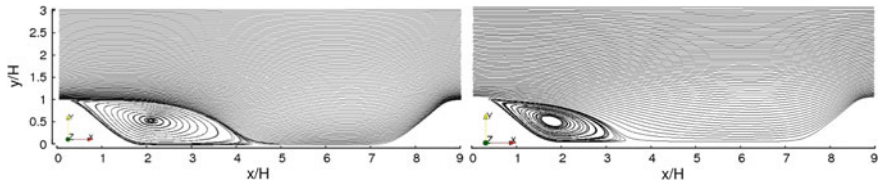


Fig. 5 Periodic flow over a 2D hill at $Re_H = 10,600$ (*left*) and $Re_H = 37,000$ (*right*)—mean streamlines obtained by the present IS-RSM

3.3 Turbulent Flow over a Backward-Facing Step

The low Reynolds number configuration ($Re_H = 5100$ based on the step height H ; the Reynolds number based on the expanding channel height is $Re_{(10H)} = 51,000$) investigated experimentally by Jovic and Driver [10] and by means of DNS by Le et al. [13] was chosen as the next test case. 1.59 Million grid cells in total were used (30

cells are distributed uniformly over the spanwise extension of $4H$). The inflow plane was located at the step wall at $-3.5H$; the solution domain is extended up to $20H$. The fluctuating field was generated by applying the method of Kornev and Hassel [11] onto the flow field obtained by the background RSM model. This configuration possesses all the features typical for a separating flow, as described in the previous section. However, as the flat plate boundary layer separates at the sharp edge (fixed separation point with the time-averaged mean dividing streamline running parallel to the step wall for a certain distance) its subsequent transformation into a shear layer is characterized by a much less intensive oscillations compared to the separation from a curved surface. Consequently, the capturing of the unsteady character of the flow is not of decisive importance for correct representation of the mean flow and time-averaged turbulence quantities. Good results could be obtained even if computing the flow in a steady manner by applying an advanced RANS model (the present Reynolds stress model is certainly such a model). The only important departure from the reference database is pertinent to a slight underprediction of the turbulence level immediately after separation similar to the separation at a curved surface (not shown here); however, unlike in the latter flow it recovers by itself leading consequently to a correct prediction of the mean reattachment length $((x/H)_{RP} = 6.28$; see the friction coefficient development in Fig. 6-lower-left). A certain weakening of the flow reversal

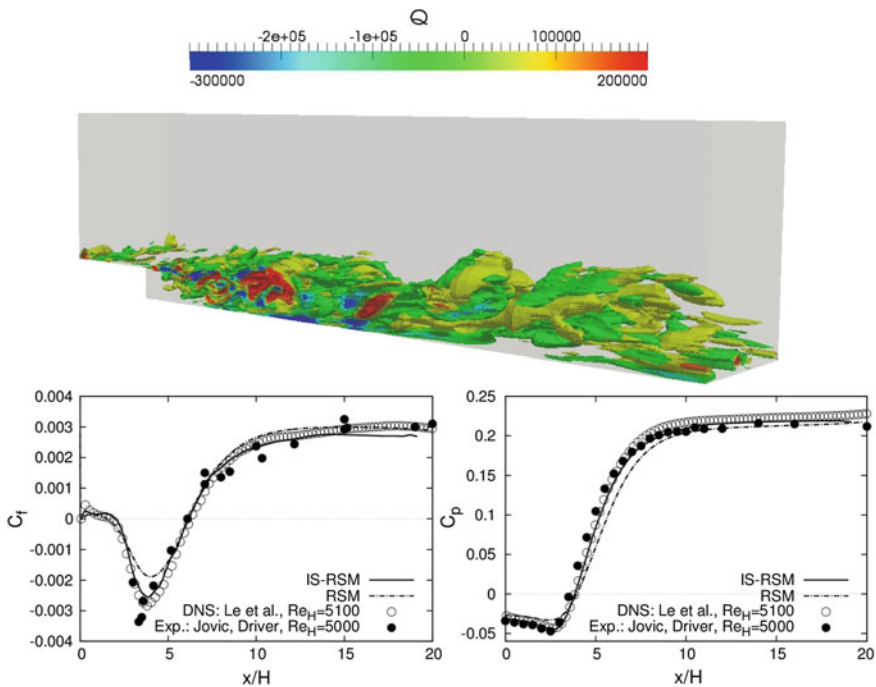


Fig. 6 Flow over a backward-facing step—vortex structure illustrated by the Q-criteria (*upper*), friction and pressure coefficients (*lower*)

intensity leads to an important underprediction of the friction coefficient magnitude whose (negative) peak coincides with the location $x/H = 4$. It is a typical RANS result pertinent especially to such a low Reynolds number. Its correct prediction (this is valid also for the pressure coefficient, Fig. 6-lower-right) requires the employment of a model being capable of capturing the instantaneous flow field. The application of the present IS-RSM model led to the vortex structure capturing (Fig. 6-upper) leading consequently to an appropriate intensification of the back-flow (not shown here) and the magnitude enhancement (negative peak) of the friction coefficient. The quality of the latter result is especially dependent on the correct capturing of the inherently unsteady impact of the near-wall streams corresponding to the mean recirculation zone and the corner bubble at the secondary reattachment point (C_f curve crosses zero value at $x/H \approx 2$).

3.4 Turbulent Flow over a Wall-Mounted Fence

The structure of the flow separated at a fence-shaped, sharp-edged obstacle mounted at the bottom wall of a plane channel is extremely complex despite the fact that the separation occurs at a fixed point coinciding with the fence tip. An impression about the flow structure complexity could be gained from Fig. 7-upper illustrating instantaneous flow field. The flow conditions upstream of the fence comply with the fluid impingement onto the fence and, consequently, with a strong upward skewing. The flow separating from the fence tip is characterized by a strongly curved, highly unsteady separated shear layer oscillating and spreading over an expanded flow region. The strong shear layer oscillations occur in a broader frequency range; the entire flow domain is dominated by large coherent structures (unlike in the case of the flat boundary layer separation from the backward-facing step, see previous section)—accordingly, the mean recirculation zone is much longer (almost two times) compared to a relevant backward-facing step configuration with $(x/H)_{RP} \approx 6 - 7$ (see the previously computed backward-facing step flow). Expectedly, these features are beyond the reach of RANS equations independent of the modeling level. The outcome is significant underprediction of the turbulence activity in the separated shear layer (see Fig. 8-lower), causing a too long recirculation zone, up to $(x/H)_{RP} \approx 14.5$ (see C_f -coefficient evolution in Fig. 7-lower).

The reference database is provided experimentally by Larsen et al. [12]. The fence-height-based ($H = 40$ mm) Reynolds number corresponds to $Re_H = 3000$ and the Reynolds number based on the channel height ($7.5H$) equals to $Re_{(7.5H)} = 22,000$. The inlet plane of the solution domain adopted is situated $8.25H$ upstream of the fence and the outlet plane is positioned at $32.5H$. The spanwise extent corresponds to $10H$. Numerical mesh comprising 1.0 Million cells in total is squeezed towards the channel and fence walls providing the dimensionless distance of the wall-adjacent grid node corresponding to $y^+ \approx 1$; the uniform distribution of 45 grid cells is adopted

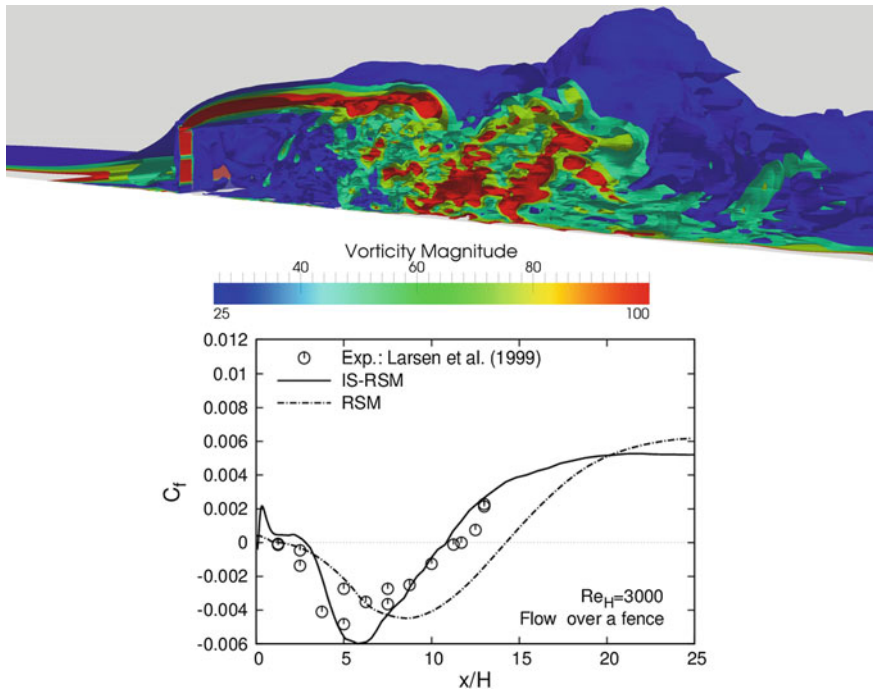


Fig. 7 Flow over a 2D fence—vortex structure illustrated by the instantaneous vorticity field (*upper*) and friction coefficient evolution at the bottom wall (*lower*)

in the spanwise direction. The RANS-RSM computations have been performed by prescribing the experimentally available velocity profile at the inflow plane. The fluctuating inflow at $-8.25H$ for the simulations using the instability-sensitive RSM model is generated by a precursor simulation of the corresponding, fully developed channel flow at $Re_{(7.5H)} = 22,000$ (with bulk velocity $U_b = 1.17$ m/s) using the same turbulence model (see Fig. 8; however, the difference in the inflow conditions is not regarded to be of decisive importance concerning the objectives of the present work dealing with the turbulence intensity enhancement being appropriately correlated with the mean velocity field).

Similarly to the case of the flow over a 2D hill important improvement is obtained by applying the IS-RSM model with the scale-supplying equation extended appropriately to account for the turbulence level enhancement in the separated shear layer region. Figure 8-lower displays the profile development of turbulent shear stress component. The improvement in the results compared to the initial Reynolds stress model is obvious. The intensified turbulence activity in the region of separation led subsequently to the separated shear layer reattachment at a distance corresponding to $(x/H)_{RP} \approx 11$ (the experimentally determined reattachment point position is at $(x/H)_{RP} = 11.7$; see also the friction coefficient development, Fig. 7-lower). This contributed strongly to the correct reproduction of the \overline{uv} profile development in its

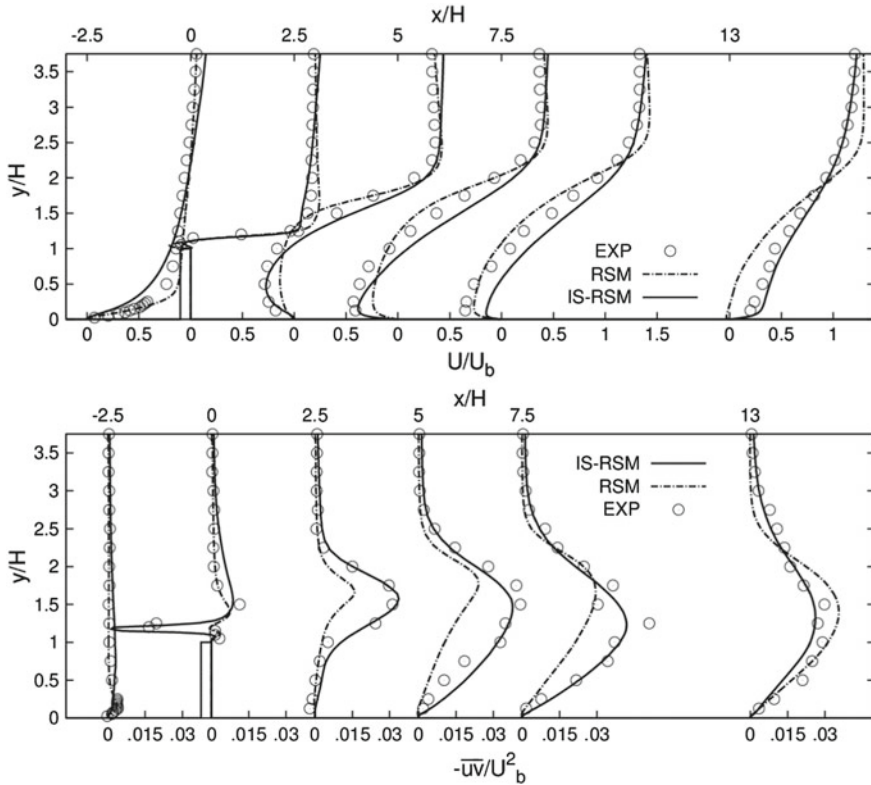


Fig. 8 Flow over a 2D fence—mean velocity (*upper*) and shear stress component (*lower*) profile developments obtained by the present IS-RSM; Exp. from [12]

entirety. The improved prediction is especially reflected in the correct capturing of the specific sign change of the shear stress component at the fence tip. The direct consequence of the correctly returned turbulent stress level increase is the greatly improved predictions of the mean velocity development, Fig. 8-upper.

3.5 Turbulent Flow in a 3D Diffuser

The flow in a presently considered three-dimensional diffuser is featured by an incompressible fully developed duct flow (height $h = 1$ cm; width $B = 3.33$ cm) discharging into a diffuser (of the length $L = 15h$), whose upper-wall and one-side wall are appropriately inclined with the expansion angles of 11.3° and 2.56° , respectively, Fig. 9-upper. The bulk velocity in the inflow duct is 1 m/s resulting in the Reynolds number based on the duct height of $Re_h = 10,000$. The reference experimental and DNS databases were provided by Cherry et al. [5] and Ohlsson et al. [17].

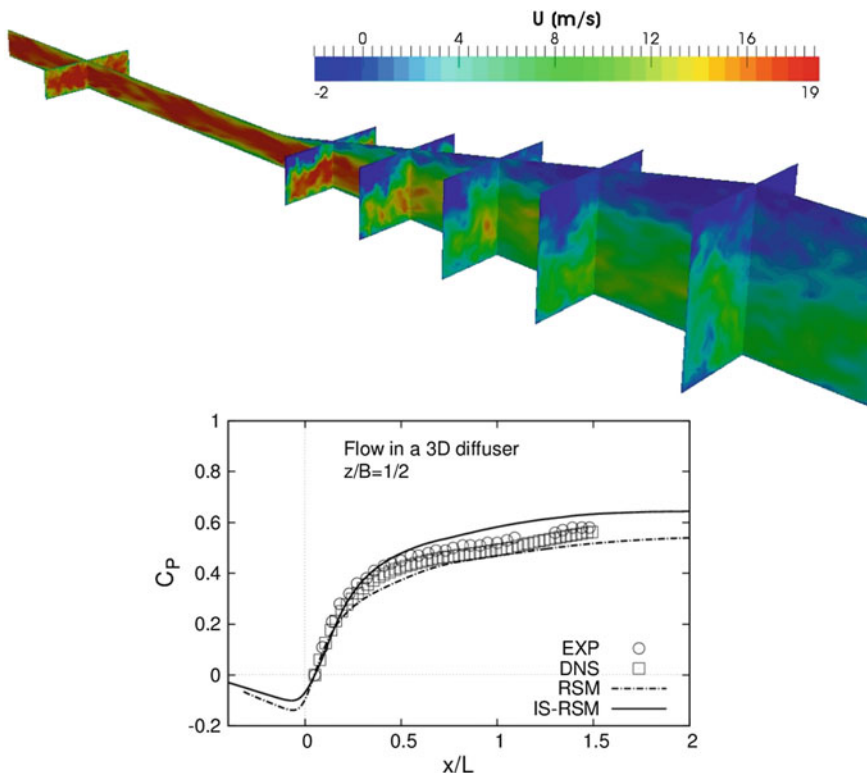


Fig. 9 Flow in a three-dimensional diffuser—instantaneous velocity field obtained by the present IS-RSM model (*upper*) and pressure coefficient development at the lower flat diffuser wall (*lower*)

The solution domain whose inlet plane is located at $x/h = -15$ (origin of the coordinate system coincides with the duct expansion onset— $x/L = 0$ —and the non-expanded side wall— $z/B = 0$) in the inflow duct and exit plane at $x/h = 45$ in the straight outflow duct was meshed with the grid consisting of 3.75 Mio. cells in total; it corresponds to the position of the wall-adjacent computational node at $y^+ \approx 1.5$. Similar to the previous 2D fence case, the fluctuating inflow was generated by performing the simulation of the fully developed flow in the 3D duct by applying the IS-RSM model.

This is a fairly complex flow characterized by the boundary layer separation starting in the corner built by two sloped walls (corner separation) and spreading over the entire upper wall (Figs. 9-upper and 10) due to an adverse pressure gradient imposed on the duct flow by expanding the cross-section area. The results obtained by the IS-RSM model are in a good qualitative agreement with the experimental findings despite a somewhat thinner recirculation zone, unlike the RANS-RSM model resulting in a growth of the corner bubble without occupying the upper wall in its entirety (not shown here). Figures 9-lower and 11 display a quantitative comparison

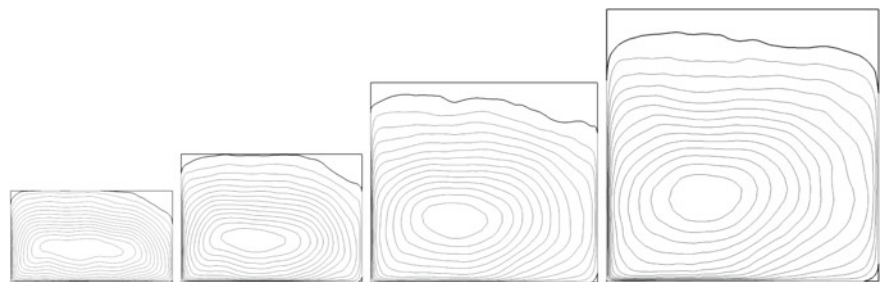


Fig. 10 Flow in a three-dimensional diffuser—iso-contours of the axial velocity field in the cross planes $y - z$ at selected streamwise locations ($x/h = 5, 8, 12$ and 15 , respectively) within the diffuser section (*thick lines* denote the zero-velocity lines) obtained by the present IS-RSM model

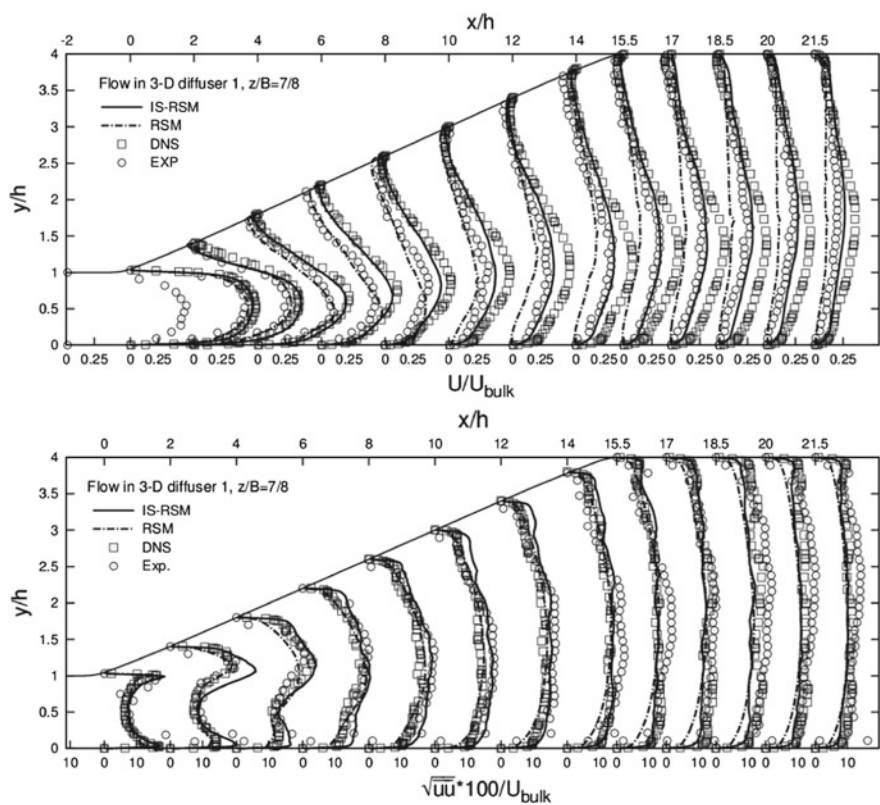


Fig. 11 Flow in a three-dimensional diffuser—evolution of the axial velocity and streamwise turbulence intensity profiles in the vertical x - y plane positioned at $z = 7B/8$. Exp. from [5, 17]

between the presently computed pressure coefficients, axial velocity and streamwise turbulence intensity profile developments and the reference experimental and DNS databases. The results obtained exhibit reasonable agreement with both data sets, especially with respect to the pressure recovery.

3.6 Flow Past Tandem-Cylinder Configurations

The presently considered pair of circular cylinders (with diameter D) in tandem (Fig. 12) represents a simplified landing gear configuration of an aircraft. The interaction between the flow fields past cylinder components was in focus of relevant experimental investigations by Neuhaert et al. [16] providing details about the mean velocity, mean surface pressure, root-mean-square of the fluctuation pressure and time-averaged turbulence intensity. Two distinct tandem-cylinder configurations characterized by different in-between spacing were considered: $L = 3.7D$ (long-distance case) and $L = 1.435D$ (short-distance case). The corresponding Reynolds and Mach numbers based on the cylinder diameter D and velocity of the oncoming flow amount 166,000 ($U_{inlet} = 1.66$ m/s) and 0.1285 respectively. The grid adopted consists of the 60,000 cells in the x - y plane for both cases. This two-dimensional grid was extended in the spanwise direction by two cylinder diameters for the IS-RSM simulations. 80 uniformly distributed grid cells were placed in the spanwise direction resulting in 4.8 Million cells in total.

According to Zdravkovich [21] the distance $L/D = 3.7$ relates to the so-called bistable case corresponding to a configuration in which the flow structure at/behind the first cylinder switches from the continuous shedding resembling the well-known von Karman vortex street to a continuously separated shear layer reattaching temporarily at the front side of the rear cylinder; behind the second cylinder a continuous vortex street develops, Fig. 12-upper-left. Unlike the long-distance case, in the short-distance configuration ($L/D = 1.435$) the cylinders are that close to each other resembling one long obstacle for the oncoming flow, Fig. 12-lower-left. Accordingly, the wall boundary layer separating quasi-stationary from the front cylinder transforms into a shear layer which reattaches at the rear cylinder. The flow in the wake behind the downstream cylinder exhibits a continuous shedding behaviour. These descriptions reveal the flow structure past the large-distance case being more challenging for turbulence models due to the bistable (intermittent) behaviour. Capturing of turbulence unsteadiness by applying the present IS-RSM model is illustrated in Fig. 1-lower displaying the field of the P_{SAS} production term. As mentioned previously, the tandem cylinder configuration can be regarded as a simplified version of a landing gear and can therefore serve as the first step in testing turbulence models for predicting the airframe noise. The unsteady pressure field is the most important flow variable acting as the noise-source representative. Conventional RANS models fail traditionally in predicting it because of their time-averaging rationale. Only unsteady interactions involving large scales can be reasonably captured. The unsteady feature of the pressure field is represented through the root-mean-square of the fluctuating

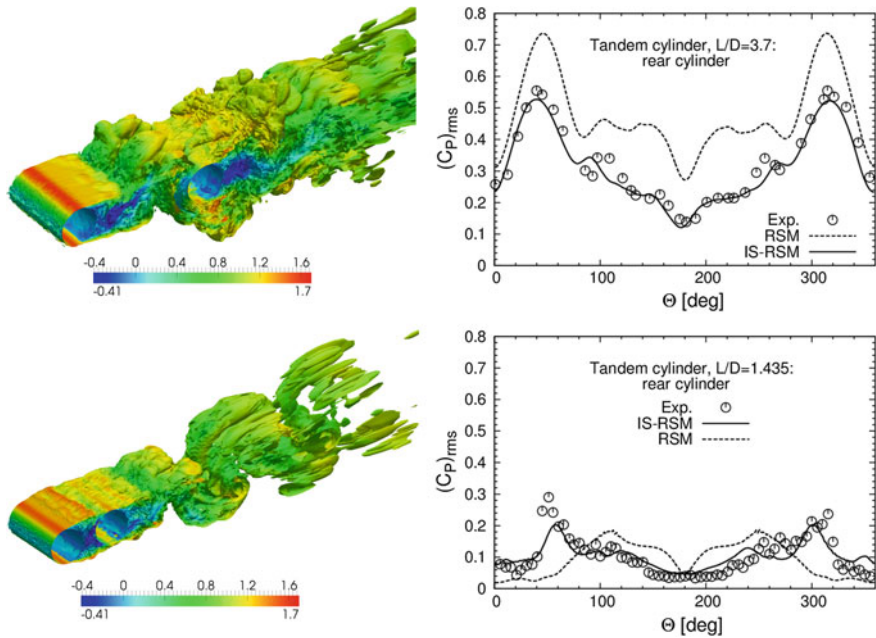


Fig. 12 Flow past tandem cylinder configurations—large ($L/D = 3.7$; *upper*) and small in-between spacing ($L/D = 1.435$; *lower*); vorticity magnitude coloured by the normalized axial velocity (U_x/U_{inlet}) obtained by the present IS-RSM (*left*) and root-mean-square (rms) of the fluctuating pressure on the downstream cylinder (*right*); Exp. from [16]

pressure on downstream cylinder for both cylinder separations, Fig. 12-right. It was experimentally found that the second cylinder is the main source of noise as the relevant $(C'_p)_{rms}$ values are four to five times higher than those measured on the upstream cylinder. Therefore, the model results compared to the experiment relate only to this downstream cylinder. The IS-RSM model results exhibit reasonable agreement in regard to both peak values and $(C'_p)_{rms}$ distribution over the most of the cylinder surface indicating high potential for being used as a tool for the noise prediction.

4 Conclusion

Potential of the presently formulated near-wall differential Reynolds stress model (RSM) extended appropriately to account for turbulence instabilities within ‘Sensitized RANS’ framework (SRANS) was illustrated by computing a series of 2D and 3D wall-bounded flow configurations featured by separation and reattachment in a broad range of Reynolds numbers. The key element in the present model is an additional SAS-based production term (in line with Menter and Egorov, [14]) introduced into the scale-determining equation governing the inverse time scale

$\omega_h (\propto \varepsilon_h/k)$. This term, formulated in terms of the ratio of the turbulent length scale to the von Karman length scale (comprising the second derivative of the velocity field), enables appropriate model receptivity to the turbulence unsteadiness promoting a selective enhancement of the turbulent dissipation rate production influencing consequently an adequate suppression of the modelled turbulence intensity towards the respective sub-scale level (related mostly to the separated shear layer region). Significantly improved predictions, compared to the baseline RSM model, with respect to the structural characteristics of the instantaneous flow field, some most important integral characteristics (e.g. friction and surface pressure coefficients), the mean velocity field and turbulence quantities demonstrate the model's potential in solving the complex flows separated from continuous curved surfaces and obstacles exhibiting broader frequency range. In addition, the capability of the model to operate in scale-resolving mode in some globally stable flows, such as flow in a plane channel and flow over a backward-facing step, is also illustrated.

Acknowledgments The work of R. Maduta has been funded by the EU project ATAAC (ACP8-GA-2009-233710).

References

1. B. Basara, S. Krajnovic, S. Girimaji, Z. Pavlovic, Partially Averaged Navier Stokes (PANS) method for turbulence simulations: near-wall eddy-viscosity transport model implementation. *AIAA J.* **49**(12), 2627–2636 (2011)
2. M. Breuer, N. Peller, Ch. Rapp, M. Manhart, Flow over periodic hills—numerical and experimental study in a wide range of Reynolds numbers. *Comput. Fluids* **38**, 433–457 (2009)
3. C.-Y. Chang, S. Jakirlic, B. Basara, C. Tropea, Predictive capability assessment of the PANS- ζ -f model of turbulence. Part I: physical rationale by reference to wall-bounded flows including separation, in *Advances in Hybrid RANS-LES Modelling 5. Notes on Numerical Fluid Mechanics and Multidisciplinary Design*, ed. by S. Girimaji, W. Haase, S.-H. Peng, D. Schwaborn (Springer, Berlin, 2015), pp. 371–383
4. B. Chaouat, R. Schiestel, A new partially integrated transport model for subgrid-scale stresses and dissipation rate for turbulent developing flows. *Phys. Fluids* **17**(065106), 1–19 (2005)
5. E.M. Cherry, C.J. Elkins, J.K. Eaton, Geometric sensitivity of three-dimensional separated flows. *Int. J. Heat Fluid Flow* **29**, 803–811 (2008)
6. J. Fröhlich, C.P. Mellen, W. Rodi, L. Temmerman, M.A. Leschziner, Highly resolved large-eddy simulation of separated flow in a channel with streamwise periodic constrictions. *J. Fluid Mech.* **526**, 19–66 (2005)
7. S.S. Girimaji, Partially-averaged Navier-Stokes model for turbulence: a Reynolds-averaged Navier-Stokes to direct numerical simulation bridging method. *J. Appl. Mech.* **73**, 413–421 (2006)
8. S. Jakirlic, K. Hanjalic, A new approach to modelling near-wall turbulence energy and stress dissipation. *J. Fluid Mech.* **439**, 139–166 (2002)
9. S. Jakirlic, R. Maduta, Extending the bounds of ‘steady’ RANS closures: towards an instability-sensitive Reynolds stress model. *Int. J. Heat Fluid Flow* **51**, 175–194 (2015). doi:[10.1016/j.ijheatfluidflow.2014.09.003](https://doi.org/10.1016/j.ijheatfluidflow.2014.09.003)
10. S. Jovic, D. Driver, Reynolds number effect on the skin friction in separated flows behind a backward-facing step. *Exp. Fluids* **18**, 464–467 (1995)

11. N. Kornev, E. Hassel, Synthesis of homogeneous anisotropic divergence-free turbulent fields with prescribed second-order statistics by vortex dipoles. *Phys. Fluids* **19**(6), 067101 (2007)
12. P.S. Larsen, J.J. Schmidt, U. Ullum, Experimental study of temporal and spatial structures in fence-on-wall test case, in *IUTAM Symposium on Simulation and Identification of Organized Structures in Flows*. Fluid Mechanics and Its Applications, vol. 52 (Kluwer Academic Publisher, 1999), pp. 25–37
13. H. Le, P. Moin, J. Kim, Direct numerical simulation of turbulent flow over a backward-facing step. *J. Fluid Mech.* **330**, 349–374 (1997)
14. F.R. Menter, Y. Egorov, The scale-adaptive simulation method for unsteady turbulent flow predictions. Part 1: theory and model description. *Flow Turbul. Combust.* **85**, 113–138 (2010)
15. R.D. Moser, J. Kim, N.N. Mansour, Direct numerical simulation of turbulent channel flow up to $Re_\tau = 590$. *Phys. Fluids* **11**(4), 943–945 (1999)
16. D.H. Neuhart, L.N. Jenkins, M.M. Choudhari, M.R. Khorrami, Measurements of the flowfield interaction between tandem cylinders. AIAA-2009-3275 (2009)
17. J. Ohlsson, P. Schlatter, P.F. Fischer, D.S. Henningson, DNS of separated flow in a three-dimensional diffuser by the spectral-element method. *J. Fluid Mech.* **650**, 307–318 (2010)
18. Ch. Rapp, M. Manhart, Flow over periodic hills: an experimental study. *Exp. Fluids* **51**, 247–269 (2011)
19. P.R. Spalart, Detached-eddy simulation. *Annu. Rev. Fluid Mech.* **41**, 181–202 (2009)
20. P.R. Spalart, W.-H. Jou, M. Strelets, S. Allmaras, Comments on the feasibility of LES for wings and on a hybrid RANS/LES approach, 1st AFOSR Int. Conf. on DNS and LES, in *Advances in DNS/LES*, ed. by C. Liu, Z. Liu (Greyden Press, Columbus, 1997), pp. 137–147
21. M.M. Zdravkovich, Flow induced oscillations of two interfering circular cylinders. *J. Sound Vib.* **101**(4), 511–521 (1985)

Progress in Wall Turbulence 2

Understanding and Modelling

Stanislas, M.; Jimenez, J.; Marusic, I. (Eds.)

2016, XI, 439 p. 273 illus., 174 illus. in color., Hardcover

ISBN: 978-3-319-20387-4